An analytical model for ballistic impacts against plain-woven fabrics with a polymeric matrix

L.M. Bresciani, A. Manes*, M. Giglio

Politecnico di Milano, Dipartimento di Meccanica, Via La Masa 1, 20156 Milano, Italy

Received 4 June 2014
Received in revised form 20 October 2014
Accepted 3 January 2015 Available online 10 January 2015

1. Introduction

Nowadays composites are employed in many applications including protection equipment capable of arresting ballistic impacts; however components may also be designed for multifunctional use, for example capable of protecting against an impact but also able to function as a load-carrying structure. Different applications also lead to different technological processes; body armours need to be resistant to impacts but also flexible, in order to adapt to the body shape: for this reason, they are made of woven fabrics, usually without a matrix. On the other hand, structural components are designed to carry load while absorbing the energy of an impact; therefore, the use of a matrix is fundamental to give the structure the required stiffness. These considerations highlight the need to fit the manufacturing of a composite structure to its end use, especially when an extreme load such as impact is possible. Although experimental tests still play an important role, modelling approaches are increasingly gaining in importance. Numerical models are a powerful tool. However, a reliable analytical methodology can be of interest in a preliminary investigation allowing the fast evaluation of several configurations. The analytical models in the literature adopt different ways of determining and approaching the fracture of the composite but all of them assume the projectile is rigid when it is made of a hard material (e.g. steel, tungsten); this hypothesis is confirmed by several experimental observations [1–3,5]. Furthermore, the analytical models reported in the

* Corresponding author.
E-*mail address:* andrea.manes@polimi.it (A. Manes).

Nomenclature

a	Yarn reference dimension
A	cross sectional area of yarns
A_{ql}	quasi-lemniscate (figure of 8) area reduction factor
a_p	deceleration of the projectile
b	wave transmission factor
C_L	longitudinal wave speed
$C_{L,Th}$	in-thickness longitudinal wave speed
C_t	transversal wave speed
E	Young modulus
$E_{bend,i}$	energy dissipated by bending of the layers
$E_{compr,i}$	energy dissipated by compression of layers
$E_{del,i}$	energy dissipated by delamination
$E_{kp,i}$	kinetic energy of the projectile
$E_{kc,i}$	kinetic energy of the moving conoid deformation
$E_{mat,i}$	energy dissipated by matrix cracking
E_{mt}	energy absorbed by matrix cracking per unit volume
$E_{py,i}$	energy dissipated by primary yarns
$E_{sy,i}$	energy dissipated by secondary yarns
$E_{sp,i}$	energy dissipated by shear plugging
E_{Th}	transversal elastic modulus
F	force on the projectile
G_{II}	critical dynamic strain energy release rate in mode II
h_1	layer thickness
L_1	length of the undeformed yarns
l_{sy}	length of deformed secondary yarns
M	bending moment per unit length
M^*	bending moment
M_c	mass of the conoid deformation
m_p	mass of the projectile
n_{failed}	number of failed layers
$n_{prop,i}$	number of layers passed by the in-thickness longitudinal wave
N_p	total number of primary yarns
n_{shear}	number of layers that undergo shear plugging
R	radius of the conoid
R_1	radius of the projectile
r_d	delamination radius
$r_{l,i}$	distance travelled by the longitudinal wave
$r_{t,i}$	distance travelled by the transversal wave
s	thickness of the deformed layer
S_{sp}	shear plugging strength
V_{mat}	matrix volume fraction
V_p	velocity of the projectile
z	depth of the conoid deformation
$z_{L,Th,i}$	distance travelled by the in-thickness longitudinal wave

Greek letters

α	angle of the conoid deformation
Δt	time step
$\varepsilon_{0,ij}$	maximum strain of the primary yarns
ε_A	compression strain of zone A
ε_B	compression strain of zone B
ρ	density
$\widehat{\rho}$	radius of camber of the deformed plate in orthogonal direction
ν	Poisson coefficient
τ_{shear}	shear stress in the target

literature employ different techniques and formulations to predict the various required ballistic parameters, including the most important, namely the residual velocity of the projectile. One of the first works on composite plates is the one of Vinson & Zukas [4], in which the analytical model is based on the propagation of longitudinal and transversal waves after the impact that generate a "V-shaped" deformation: after reaching a threshold strain value, the composite is considered broken. The velocity is not derived from the energy balance of the several dissipation modes but from calculation of the resistance force of the plate. Roylance [7] and Field & Sun [8], exploited, the longitudinal and transversal wave propagation theory to obtain the strain in the fibres and hence a relationship with the impact velocity, to define a design optimization methodology. In Ref. [6] the calculation of the velocity of the projectile is based on momentum equations that link the strain along the yarns with the velocity itself, basing the model on previous studies on single yarn impacts [8]; furthermore, it considers combined failure criteria depending on the tensile and shear stress and it reproduces multi-layers targets without a matrix. The analytical models based on the energy balance to derive the deceleration of the projectile give an accurate understanding of how the kinetic energy of the projectile is dissipated and which dissipation mode prevails over the others, thus pointing the focus of the design on the relevant parameters. In Ref. [2] three major components i.e. the tensile failure of the composite, the elastic deformation and the kinetic energy of the moving conoid of the composite were identified to contribute to the energy lost by the projectile during the ballistic impact. The most dominant energy absorbing mechanism was found to be the kinetic energy of the deforming composite. In Ref. [1] further components were added to the energy balance: deformation of the primary and secondary yarns, delamination, matrix cracking and shear plugging. The strain in the composite is hypothesized to decrease linearly through the thickness, but how the gradient of the slope is identified is not explained; also, shear plugging is reproduced assuming that the whole force to which the projectile is subjected acts on the cylindrical surface of the target around the tip of the blunt projectile. In the present work, the analytical model adopts an energy balance to derive the velocity and the wave propagation theory studied in earlier works [1,2,7,9,10] forms the base. This choice was made to develop an accurate model capable of working correctly over a wide range of conditions, from the thickness of the target and its materials, to the variation of the impact velocity, the mass and dimensions of the projectile, which is however constrained to be a rigid body with a cylindrical blunt shape (BSP). To achieve this, the reference models cited above were studied and changes made, especially broadening the working range of the model. The main parameter of interest remains the residual velocity, to provide the ballistic limit of the projectile-target couple, because this limit is the ultimate indicator of the effectiveness of ballistic protection. In Section 2, the formulation of the model is presented. In each paragraph the different dissipation modes are described: the kinetic energy of the "V-tent" deformation, the energy of the yarns under tensile strain, the energy required to bend the composite plate, the compression of the layers, the delamination and the matrix cracking and finally shear plugging. In Section 3, the analytical model is compared and validated with experimental data obtained by the authors [5] along with other data from the literature; in particular, the residual velocity and the ballistic limit for different target materials and thickness are analysed, but also the energy trend in time and the morphological features are investigated.

2. Analytical model

The analytical model in the present work reproduces normal impacts of rigid blunt projectiles against composite woven fabric targets impregnated in a polymeric matrix. The model is implemented in Matlab® and is based on the wave propagation theory presented in the literature [1,2,7,9,10]. The velocity of the projectile is obtained at every time-step from the energy balance. Additional contributions have been introduced with the aim of broadening the working range of the model itself and the number of energy dissipation modes. The projectile is modelled as a rigid body. The energy balance considers that the composite target absorbs the initial kinetic energy of the projectile, under different modes that can be summarised as:

$$E_{kp,0} = E_{kp,i} + E_{kc,i} + E_{py,i} + E_{sy,i} + E_{bend,i} + E_{compr,i} + E_{del,i} + E_{mat,i} + E_{sp,i} \quad (1)$$

where $E_{kp,0}$ is the initial kinetic energy of the projectile, $E_{kp,i}$ is the kinetic energy of the projectile at every time step, $E_{kc,i}$ is the kinetic energy of the composite cone ahead the tip of the projectile, $E_{py,i}$ and $E_{sy,i}$ are the energies absorbed by primary and secondary yarns, $E_{bend,i}$ is the energy due to the bending of the plate under the action of the projectile, $E_{compr,i}$ is the energy absorbed by the compression of the layers under the penetration of the projectile, $E_{del,i}$ and $E_{mat,i}$ are the energies absorbed by the delamination among the layers and the cracking of the matrix and $E_{sp,i}$ is the energy dissipated by plugging of the layers, if this phenomenon takes place. The main hypotheses at the base of the model are:

- Normal impacts
- No creep or stress relaxation
- Rigid blunt shaped projectile
- Constant thickness of the layers in time
- No wave attenuation with distance
- When longitudinal in-plane wave stretches the yarns, section reduction is neglected
- Friction neglected

According to the wave theory presented in Refs. [1,2,7,9,10], when a projectile impacts the yarns, two waves propagate along them; the longitudinal wave has the highest velocity and its equation is:

$$C_L = \sqrt{\frac{E}{\rho}} \quad (2)$$

As the strain wave passes a given point on the yarn, material flows inwards towards the impact point. The material in the wake of the wave front forms itself into a transverse wave, shaped like an inverted tent with the impact point at its vertex. In a fixed coordinate system with the origin on the circumference of the projectile tip, the base of the tent spreads outwards with the transverse wave velocity. The transverse wave velocity [1] is given by:

$$C_t = \sqrt{\frac{(1+\varepsilon_p)\sigma_p}{\rho}} - \int_0^{\varepsilon_p} \sqrt{\frac{1}{\rho}\left(\frac{d\sigma}{d\varepsilon}\right)}\, d\varepsilon \quad (3)$$

where ε_p and σ_p are the strain and stress threshold before plastic behaviour occurs. Knowing the velocities of the waves, the distances travelled by them in a finite interval of the time Δt can be obtained, where $r_{t,i}$ corresponds to the radius of the base of the composite conoid deformation and $r_{l,i}$ the distance travelled by the longitudinal waves.

$$r_{l,i} = \sum_0^i C_L * \Delta t \quad (4)$$

$$r_{t,i} = \sum_0^i C_{t,n} * \Delta t \quad (5)$$

2.1. Sequential failure of the layers

The impact of the projectile against the target causes the propagation of longitudinal and transverse waves that spread along the surface of the target, as described before, but this phenomenon takes place also through the thickness of the plate, which is the penetration direction [11]. The in-thickness longitudinal wave (travelling through the thickness of the plate), has a higher velocity, and is responsible for the bulge formation in the layers. As shown in Ref. [5] experimentally and with numerical simulations, in the very first instants, when the projectile comes into contact with the first layer, the rear layers are still undeformed and a bulge is not observed. As soon as the longitudinal wave reaches the layers on the rear, these start moving in the direction of the projectile penetration and when the wave has reached the last layer, a bulge can be observed and therefore the spread of the "V-shaped" deformation takes place in the whole plate. Starting from these observations, a formulation that reproduces the sequential failure of the layers that occurs during as the projectile advances, was developed and implemented. The sequential propagation of the stress waves and the consequent failure of the layers allows the determination of the number of non-perforated layers at impact velocities around the ballistic limit, which is a borderline situation in protection design. The idea at the base is that at the first instant, when the projectile comes into contact with the target, the in-plane transverse and longitudinal waves, and the in-thickness longitu-dinal wave start spreading. For the first two waves formula for their wave speed has been given earlier, in the following the model for the propagation through the thickness is presented.

$$C_{L,Th} = \sqrt{\frac{E_{Th}}{\rho}} \quad (6)$$

The velocity of the longitudinal wave through the thickness is given by Eq. (6), where E_{Th} is the transverse elastic modulus of the composite, which is assumed homogeneous, as ρ remains unchanged. The distance travelled by this wave is therefore given by:

$$z_{L,Th,i} = \sum_{n=0}^{n=i} C_{L,Th} * \Delta t \quad (7)$$

From this equation, the number of layers through which the wave has propagated is derived knowing the thickness h_1 of a single layer:

$$n_{prop,i} = floor\left(\frac{z_{L,Th,i}}{h_1}\right) \quad (8)$$

At the first time step, the in-plane longitudinal and transversal waves propagate in the first layer, and the in-thickness longitudinal wave starts propagating. As the projectile advances, the first layer undergoes the "V-tent" deformation while the rear layers are still undeformed. When the wave reaches a new layer, the hypothesis is made that in-plane transversal and longitudinal waves propagate

in that layer, according to Equations (2) and (3). When the in-thickness wave reaches a new layer, it starts moving along the penetration direction at the same speed as the previous layer that is pushing it, and it in turn starts pushing the following layer that is still undeformed. Every layer therefore consecutively undergoes the formation of the "V-shaped" deformation, which induces strain in the yarns, as described below. This mechanism continues until the wave reaches the rearmost layer. From that moment on all the layers move at the speed of the projectile and undergo strain and stress leading to possible failure. The longitudinal wave reflects from the rear free surface, but the physical effects of this phenomenon are neglected in this model. Fig. 1 shows the steps of the mechanism described, to give a better understanding.

2.2. Dissipation energies

The impact of the projectile causes the propagation of the waves and therefore stress and strain are generated in the woven yarns. The primary yarns are those in direct contact with the projectile tip (and in the layers beneath it) and undergo the highest strains, while all the other deformed yarns are categorized as secondary yarns that undergo a lower strain [1]; the details of these formulations are provided in the following sections.

In addition, part of the kinetic energy of the projectile is absorbed by the "V-tent" deformation that moves along the projectile's trajectory and increases its mass together with the radius that is given by the distance travelled from the in-plane transverse wave (Eq. (5)). Since the deformation of the composite plate has a conoid shape, a formulation of the bending energy has been developed, based on the thin circular plate theory. This formulation is an additional contribution of the present paper to broaden the working field of the model, with the aim to extend the analysis to thick plates. The other energies, added as additional contribution, are related to compression of the layers under the action of the projectile, delamination between layers, matrix cracking and shear plugging. The different modes of energy absorption by the composite target are discussed in detail in the following section.

2.2.1. Energy absorbed by primary yarns

The formula to calculate the energy dissipated by the deformation of the primary yarns, which are in direct contact with the tip of the projectile (and in the layer beneath it), is derived from Ref. [1]. The decrease of the wave energy given by the material damping makes the strain along the yarns not constant along their length, but it drops from the tip of the projectile, where it has a maximum, to the limit of the propagation of the longitudinal wave, according to a negative exponential law, shown in Eq. (9). Similar behaviour was found also in Ref. [12].

$$\varepsilon(x)_{ij} = \varepsilon_{0,ij} b^{\frac{x}{a}} \tag{9}$$

Here ε_0 is the strain at position x = 0, that is at the tip of the projectile, a is the yarn size and b is a constant of magnitude less than 1, that represents the transmitted component of the stress wave, hence it is called transmission factor; it is strongly dependent upon the geometry of the fabrics as well as their mechanical and physical properties [1,15]. The value of the strain ε_0 is obtained by integrating differential equations, derived from the equilibrium of a deformed composite yarn and it changes layer by layer according to the propagation of the waves:

$$\varepsilon_{0,ij} = \left[\frac{\sqrt{r_{t,ij}^2 + z_{ij}^2} - r_{t,ij}}{b^{\frac{L_1}{a}} - 1} \right] \frac{\ln b}{a} \tag{10}$$

where L_1 is the initial length of the yarn and z the depth of the composite conoid deformation. Knowing the stress-strain curve of the material of the fibres, the energy absorbed by the deformed primary yarns can be evaluated by integrating the area under the curve giving the energy per unit of volume, then integrating it up to the distance travelled by the longitudinal wave responsible for the tension stress:

$$E_{py,ij} = 2N_p A \int_0^{r_{l,ij}} \left(\int_0^{\varepsilon_0 b^{\frac{x}{a}}} \sigma(\varepsilon) d\varepsilon \right) dx \quad [J] \tag{11}$$

where N_p is the total number of primary yarns in a single layer and the factor of 2 is due to the symmetry of the problem. Since in the first instance the in-thickness wave has not propagated through all the layers, as explained in the previous section, not all of them undergo tension and dissipate energy. In addition, the strain

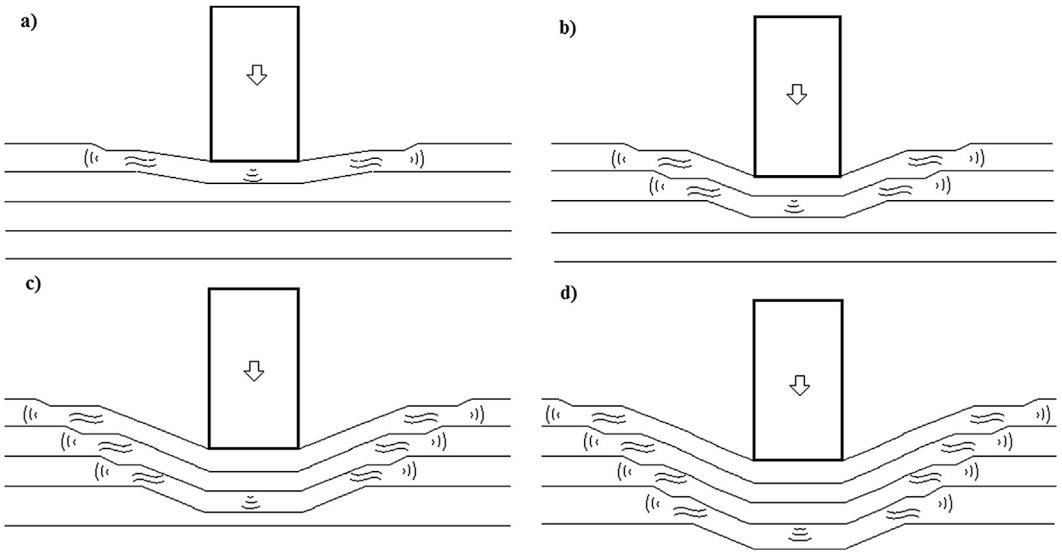

Fig. 1. Steps of the projectile penetration with sequential "V-tent" deformation and bulge formation.

changes from layer to layer according to the different radii of the in-plane longitudinal and transversal waves. Therefore, the total energy absorbed by the deformed primary yarns is the sum of those of the j-deformed layers at every i-th time step:

$$E_{py\_tot,i} = \sum_{j=0}^{n_{prop,i}} E_{py,ij} \tag{12}$$

The process of energy absorption proceeds until the maximum strain ε_0 reaches the failure threshold value, which means that the primary yarns of the j-th layer fail.

2.2.2. Energy absorbed due to the deformation of secondary yarns

The modelling of the energy absorbed by the secondary yarns differs from the Naik & Shrirao modelling [1], in which the region composed by secondary yarns is modelled as a continuous mean, neglecting the yarns that are discrete and separated. In Ref. [1] the approach is based on imposing a linear radial gradient of the strain, which is independent from the angular coordinate. Instead, the new formulation considers discrete yarns, basing the evaluation of the energy absorbed by each yarn on the theory of the stress wave attenuation, presented for the primary yarns. Fig. 2 shows the idea at the base of this modelling approach: the evolution of the strain along the primary yarns imposes on the secondary yarns a strain that is also related to the V- tent deformation. The primary yarns are discretized with a vector:

$$\overline{x} = [x_1, x_2, x_3 \ldots\ldots\ldots x_n] \tag{13}$$

The height of the conoid is evaluated for every x_j, therefore the maximum strain of every secondary yarn that is assumed to follow the "V-tent" deformation of the layer can be calculated by:

$$\varepsilon_{0,sy} = \left[\frac{\sqrt{l_{sy}^2 + z(x_j)^2} - l_{sy}}{b^{\frac{L_1}{a}} - 1} \right] \frac{\ln b}{a} \tag{14}$$

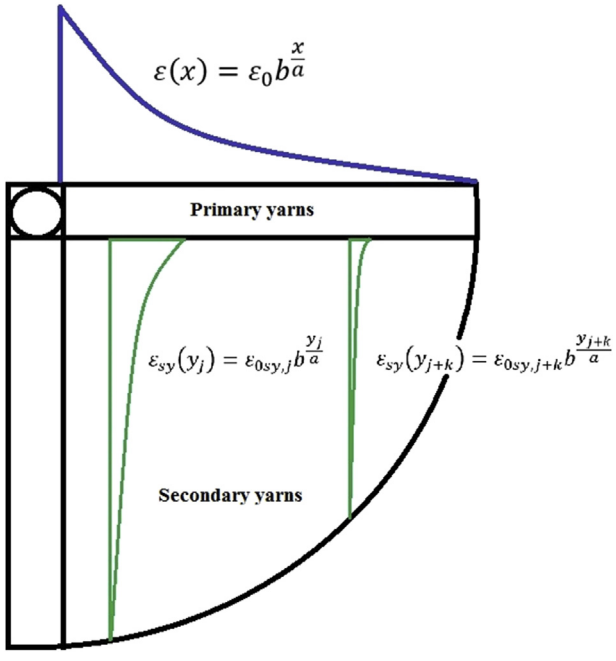

Fig. 2. Stress attenuation wave in primary and secondary yarns, according to the new formulation.

The length of the secondary yarns l_{sy} is evaluated for every yarn and layer at every time step as follows:

$$l_{sy} = \sqrt{r_t^2 - x_j^2} \tag{15}$$

Hence, the evolution of the strain along the secondary fibres, that are assumed to be perpendicular to the primary ones, follows the exponential law presented in the wave stress attenuation theory, only changing ε_0 with $\varepsilon_{0,sy}$. Every secondary yarn has a different length, resulting in a different maximum strain. Finally, the energy absorbed by the deformation of the secondary yarns in the j-th deformed layer is given by:

$$E_{sy,ij} = 4 \sum_{1}^{n} 2A \int_{0}^{l_{sy}} \left(\int_{0}^{\varepsilon_{0,sy} b^{\frac{y_j}{a}}} \sigma(\varepsilon) d\varepsilon \right) dy \quad [J] \tag{16}$$

where the term in the summation is the energy of a single yarn. The factor of 4 is due to the symmetry of the problem and to the perpendicular weaving of secondary yarns. The coordinate system for the calculation of the integrals is put on the circumferential edge of the projectile. The energy dissipated by the secondary yarns changes from layer to layer according to the propagation of the waves and the resulting travelling distance, the total energy is the sum of them all.

2.2.3. Kinetic energy of the composite "V-shaped" deformation

When the projectile impacts the composite target, the in-plane transverse wave generates a conoid deformation that moves forward together with the projectile, with the same velocity at the tip: therefore, part of the kinetic energy of the projectile is transformed into its kinetic energy. From the experimental observations [7], the cone moves forward at the same velocity of the tip of the projectile that is in contact with it: the velocity from the tip to the base of the V-tent deformation does not vary, so the angle with the surface remains constant. As the in-thickness longitudinal wave proceeds, the sequential "V-tent" deformation takes place also in the following layers (Fig. 1) and so the expression of the kinetic energy dissipated by the deformed layers is:

$$E_{kc} = \sum_{j=1}^{n_{prop,i}} \frac{1}{2} M_{c,ij} V_{p,i}^2 \tag{17}$$

where $M_{c,\ ij}$ is the mass of the moving conoid in every layer that depends on the thickness, the density of the target and the radius given by the transverse waves distance.

2.2.4. Energy absorbed due to bending of the layers

The penetration of the projectile causes bending of the layers, with an angle that is dependent upon the speed of the projectile itself and on the distance travelled by the in-plane transverse waves. The following formulation is based on the thin plate theory, making some extra assumptions: the thickness of every layer remains constant, the material is considered homogenous, perfectly linear and isotropic, and the plate is subjected to a plane-stress configuration.

Considering a thin plate subjected to out of plane displacements (w), the equations that describe the in-plane state of strain of the plate are given by the system of the Equation (18), where $\widehat{\rho}$ is the radius of camber of the plate in the orthogonal directions:

$$\begin{cases} \varepsilon_x = -z\dfrac{d^2w(x,y)}{dx^2} = -z\dfrac{1}{\rho_x} \\ \varepsilon_y = -z\dfrac{d^2w(x,y)}{dy^2} = -z\dfrac{1}{\rho_y} \\ \gamma_{xy} = \dfrac{du}{dy} + \dfrac{dv}{dx} = -2z\dfrac{d^2w(x,y)}{dxdy} \end{cases} \tag{18}$$

Exploiting the stress–strain relationships given for a plane-stress configuration of the plate (σ_z=0), the stresses can be integrated to obtain the resistant moments per unit length:

$$\begin{cases} M_x = \int_{-\frac{s}{2}}^{\frac{s}{2}} \sigma_x z dz = -\dfrac{Es^3}{12(1-\nu^2)}\left(\dfrac{1}{\rho_x} + \nu\dfrac{1}{\rho_y}\right) = D\left(\dfrac{1}{\rho_x} + \nu\dfrac{1}{\rho_y}\right) \\ M_y = \int_{-\frac{s}{2}}^{\frac{s}{2}} \sigma_y z dz = -\dfrac{Es^3}{12(1-\nu^2)}\left(\dfrac{1}{\rho_y} + \nu\dfrac{1}{\rho_x}\right) = D\left(\dfrac{1}{\rho_x} + \nu\dfrac{1}{\rho_y}\right) \quad \left[\dfrac{Nm}{m}\right] \\ M_{xy} = \int_{-\frac{s}{2}}^{\frac{s}{2}} \tau_{xy} z dz = -2G\dfrac{s^3}{12}\dfrac{d^2w(x,y)}{dxdy} \end{cases} \tag{19}$$

The first two moments per length are of interest in this treatise, the third is the in-plane torque that is neglected in the formulation of the bending moments of the plate. Assuming that the "V-tent" deformation imposed by the penetrating projectile has a round shape at the base, the cambers in the x and y directions as well as the bending moments are therefore identical.

Fig. 3 shows the sketch of the deformation imposed by the projectile that is equivalent to stating that the displacement "*f*" is imposed along the direction perpendicular to the plate. On the basis of what was previously said that the cambers of the plate are the same, the resistance moments become:

$$M_x = M_y = M = D\left(\frac{1}{\widehat{\rho}} + \nu\frac{1}{\widehat{\rho}}\right) \tag{20}$$

And so:

$$\begin{cases} \alpha = \dfrac{R}{\widehat{\rho}} = \dfrac{MR}{(1+\nu)D} f = \dfrac{(2R)^2}{8\widehat{\rho}} = \dfrac{MR^2}{2(1+\nu)D} \end{cases} \tag{21}$$

From one of the equations in system 21 the moment per unit length M is derived and by multiplying it by the circumference, the resistance moment acting on the circumference of the "V-tent" deformation of every layer is obtained (Eq. (22)). Finally, the energy dissipated to impose the bent configuration of the plate is derived by multiplying it by the angle of the conoid (α) (Eq. (23)).

$$M^* = 2\pi R^* \frac{f 2(1+\nu)D}{R^2} \quad [Nm] \tag{22}$$

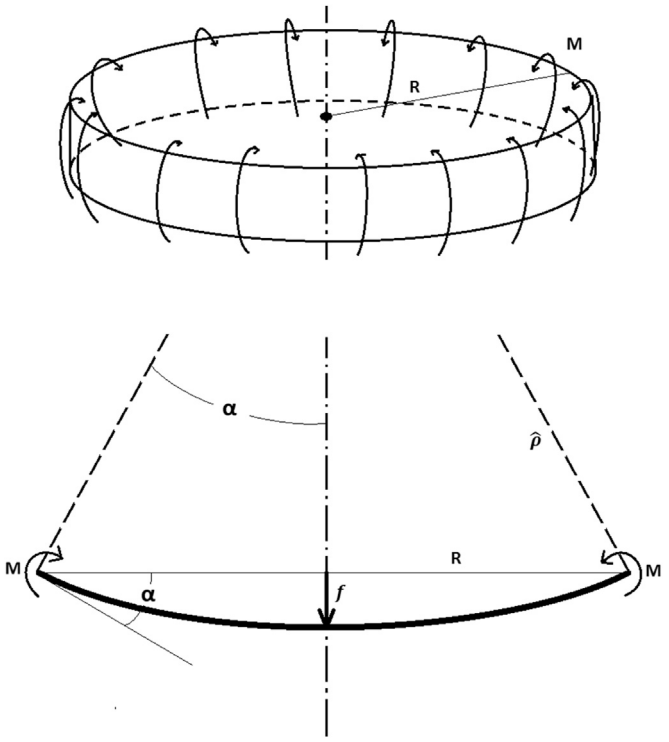

Fig. 3. Representation of circular deformation with imposed displacement in the z direction.

$$E_{bend,i} = M^* \alpha \quad [J] \tag{23}$$

2.2.5. Energy absorbed due to compression of the layers

When the projectile penetrates the target, every layer subjected either to the action of the projectile directly or to the intervening layers, undergoes a compression strain until the longitudinal in-thickness wave has reached the rearmost layer. This strain is highest at the tip of the projectile and decreases to zero up to the radius of the in-plane transversal wave.

The compressed volume presents the zone "A" that has a constant compression strain along the radius, while in the zone "B" the compression strain depends linearly upon the radial coordinate.

$$\varepsilon_A = \frac{z}{h} \tag{24}$$

$$\varepsilon_B(r) = \frac{\varepsilon_A}{r_t} r \tag{25}$$

The energy absorbed by the compression of one layer is therefore:

$$E_{compr} = \pi R_1^2 h \int_0^{\varepsilon_A} \sigma(\varepsilon) d\varepsilon + \int_0^{r_t}\int_0^{\varepsilon_B} \sigma(\varepsilon) d\varepsilon \, 2\pi r h \, dr \quad [J] \tag{26}$$

The sum of the energies absorbed by all the layers that are compressed in time, gives the total compression energy.

2.2.6. Energy absorbed due to shear plugging

As explained in Ref. [5], in the first instance of the impact, high transverse shear forces are observed in the first layers along the circumference of the projectile, while as the projectile penetrates, the rear layers undergo high in-plane tension stresses and lower

shear forces. The impulsive phenomenon in the first time steps causes the failure of the layers by shear plugging that is the formation of a cut disc equal to the dimension of the blunt projectile tip. The formulation of this mode of energy dissipation is an improvement of the one presented in Ref. [1] and is linked to the modelling of the sequential failure and propagation of the in-thickness shock waves. The projectile's force on the target generates shear stresses along the perimeter of the projectile itself, but in the very first instance, the force is not distributed over the entire thickness, because the in-thickness longitudinal wave, responsible for the bulge formation, has not propagated up to the rear layer. In fact, the layers that are not exposed to the passage of the shock wave are not even subjected to the action of the projectile, since they are not moving with it (Fig. 1). As the wave propagates towards the rear layers, the shear force is distributed over a wider area, involving several layers and consequently the shear force decreases. The equations describing this phenomenon are the following:

$$F = m_p a_p = m_p \frac{\Delta V}{\Delta T} \tag{27}$$

$$\tau_{shear} = \frac{F}{2\pi R h_1 n_{shear}} \tag{28}$$

The deceleration of the projectile multiplied by its mass, gives the force on the projectile that is equal to the force applied to the target generating the shear stresses. When the shear stress overcomes a threshold shear stress S_{sp}, the layers involved in the shear plugging fail. The shear force is applied to the layers that have undergone the passage of the in-thickness longitudinal wave and that have not yet failed because of the shear plugging or the reaching of the threshold strain limit due to tensile stress in the yarns. Hence, the number of layers involved in shear plugging at every time step is given by:

$$n_{shear} = n_{prop} - n_{failed} \tag{29}$$

If no layers fail, all of them are involved in the absorption of the shear stress, which is consequently lower and for this reason the rear layers are less subject to this phenomenon. If the layers are broken under the shear plugging conditions, then the energy dissipated is given by:

$$E_{sp} = S_{sp} n_{shear} 2\pi R h_1^2 \tag{30}$$

2.2.7. Energy absorbed due to delamination and matrix cracking

Delamination and matrix cracking absorb some part of the initial kinetic energy of the projectile. Only part of the layers interface undergoes delamination and matrix cracking, and, complete matrix cracking is unlikely to occur. Evidence for this phenomenon is provided by the fact that after ballistic impact, the matrix is still attached to the fibres and is not completely separated from the reinforcement [1]. The area of delamination and matrix cracking is given by:

$$A = \pi\left(r_{d(i+1)}^2 - r_{d,i}^2\right) A_{ql} \tag{31}$$

where r_d is the radius up to which the damage has propagated and A_{ql} is a scale factor to account for the fact that the delaminated area usually shows a quasi-lemniscate shape (figure of 8) [1]. Therefore, the energies absorbed by delamination and matrix cracking during a time interval are given by:

$$E_{del,i} = E_{del\cdot(i-1)} + P_d \pi\left(r_{d(i+1)}^2 - r_{d,i}^2\right) A_{ql} G_{II} \tag{32}$$

$$E_{mat,i} = E_{mat\cdot(i-1)} + P_m \pi\left(r_{d(i+1)}^2 - r_{d,i}^2\right) A_{ql} E_{mat} h V_{mat} \tag{33}$$

P_d and P_m stand for the percentage of delamination and the percentage of matrix cracking, G_{II} is the threshold energy before delamination, E_{mat} is the same thing for the matrix cracking; V_{mat} is the percentage in volume of the matrix. Fig. 4.

2.3. Projectile velocity

Once all the energies have been calculated, the velocity of the projectile is derived from the energy balance (1):

$$V = \sqrt{\frac{E_{kp,0} - \left(E_{py} + E_{sy} + E_{kc} + E_{bend} + E_{compr} + E_{sp} + E_{del} + E_{mat}\right)}{\frac{1}{2}\left(m_p + M_c\right)}} \tag{34}$$

The programme ends if all the composite layers fail or if the projectile has zero residual velocity.

3. Results and validation

The main parameter used to assess the accuracy of the model, is the predicted residual velocity of the projectile, which is compared with the experimental results from Ref. [5] for Kevlar29/Epoxy composite targets with different thicknesses (5–10 mm) and with other experimental data from the literature that involve other materials such as glass fibres [1,16], and a thickness up to 20 mm. Additional parameters like the dimensions of the "V-tent" deformation and the evolution in time of the several modes of energy dissipation are also analysed to better understand which parameter contributes most. The input parameters of the model are essentially the mechanical properties of the composite target, starting from the stress-strain curve that allows the evaluation of the energy absorbed by the tension and compression of the composite together with the wave transmission factor *b*. The number of layers, the shear plugging strength, the parameters related to delamina-tion and matrix cracking and the dimensions and mass of the projectile complete the list of input parameters.

3.1. Residual velocities

The most important parameter for assessing ballistic protection design is the residual velocity of the projectile after the impact, and from this the ballistic limit of the couple projectile-target. This velocity represents the capability of the target to absorb energy, which rises along with the ballistic limit. Figs. 5 and 6 show the comparison of the predicted residual velocity of the projectile at

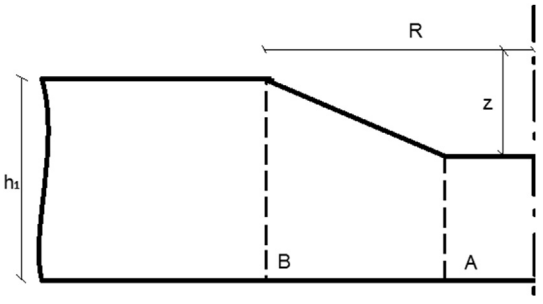

Fig. 4. Compression of a single layer.

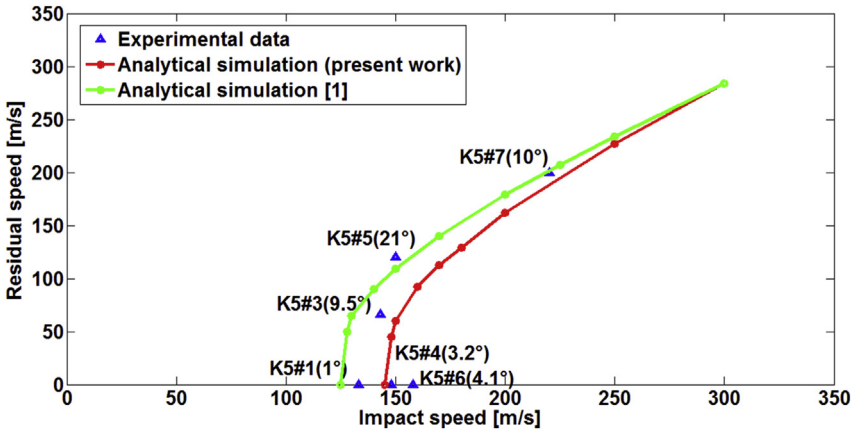

Fig. 5. Comparison of residual velocities with [5]: 5 mm plate.

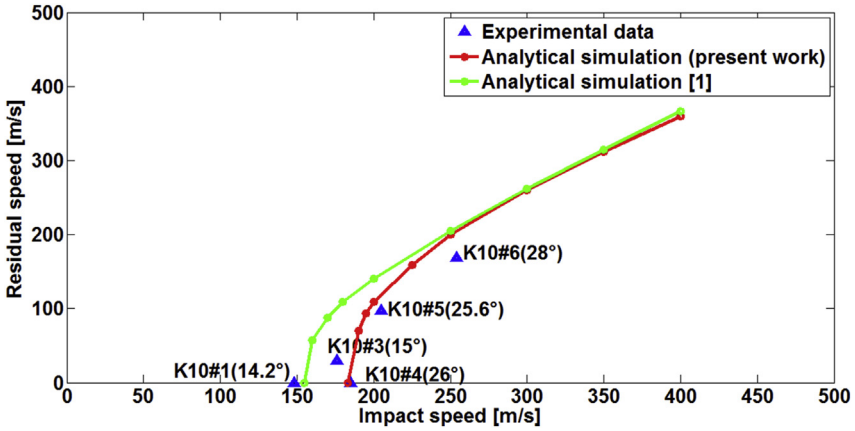

Fig. 6. Comparison of residual velocities with [5]: 10 mm plate.

different impact velocities with the experimental data obtained in another study by the authors [5]. It's worth underlining that the experimental values are also affected by an unexpected experimental variability due to a non-null impact Yaw angle (the value between brackets in figures) whereas the analytical model considers a perfect perpendicular situation. For blunt projectiles, the perforation capability increases together with the Yaw angle, for values up to about 20°, while it presents a reversal of tendency around 30°, as explained in Ref. [5]. The input parameters to the analytical model come from Refs. [1,3,5,13,14,18] and are summarised in the following table. Table 1.

No value of the wave transmission factor regarding the Kevlar® is published in the literature and hence a value of 0.9 was chosen starting from physical considerations concerning the values of other materials, in particular E-glass and Carbon fibres that are available in the literature. The chosen value lies between the lower value of the E-glass and the higher value of the Carbon T-300 presented in Refs. [13]; since this parameter represents the capability of the materials to dissipate energy by means of spreading out of the waves, it is related to the Young modulus and density of the material. The properties of Kevlar® lie between the values for Car-bon (upper) and E-glass (lower). Comparison of the analytical re-sults shows that the analytical curves have a linear behaviour at high impact speeds and a marked “bend” close to the ballistic limit, similar to the experimental values. Figs. 5 and 6 highlight the difference between two analytical models. The model implemented according to [1] does not reproduce the compression and bending energies that seem to have an important influence on the prediction of the residual velocity of the projectile. Also it modelled the secondary yarns energy absorption without discretization of them. Implementation of the present model increases the ballistic limit for both the 5 and 10 mm plates and leads to a better fitting of the overall results with the 10 mm specimen, which is subjected to

Table 1
Projectile and target input features for comparison with [5].

Projectile tungsten BSP	
L [mm]	20
D [mm]	10
$\rho\ \left[\frac{kg}{m^3}\right]$	19,300
Target Kevlar®29/Epoxy	
N° layers	12/24
Thickness [mm]	5/10
ε_f [%]	3.84
E [GPa]	82
$\rho\ \left[\frac{kg}{m^3}\right]$	1440
Ssp [MPa]	898
$G_{II}\ [J/m^2]$	1000
$E_{mt}\ [J/m^3]$	900,000
b	0.9
V_{mt} [%]	50
Yarn width [mm]	1.2
Yarn height [mm]	0.25

Table 2
Target input features for the comparison with [1,16].

Target E-glass/vinylester	
ε_f [%]	4.4
E [GPa]	72
$\rho\left[\frac{kg}{m^3}\right]$	1750
Ssp [MPa]	650
G_{II} [J/m^2]	1000
E_{mt} [J/m^3]	900,000
b	0.875
V_{mt} [%]	50

bending and compression by a higher degree. At high impact velocities, the difference between the residual velocities of the two models is smaller; the reason for this is investigated through the energies dissipation mechanism in the following section. Close to the ballistic limit, the model in the present paper predicts residual velocities that are close to the experimental values.

The current improved analytical model for the 10 mm plate shows excellent agreement with the experimental values reported in Refs. [5], accounting for the variance of the experimental data near the ballistic limit, where the predicted residual velocities (red line) fit the experimental values much better than at low residual velocities. The ballistic limit predicted by the current analytical model is 148 m/s for the 5 mm plate and 185 m/s for the 10 mm plate; both these values are in close agreement with the experimental ballistic limit reported in Ref. [5] that are 143 m/s and 176 m/s respectively.

In the following, the model is also compared with data from the literature, to verify its reliability for different materials and thicknesses of the composite target. In Refs. [1,16] the experimental tests were carried out on E-glass composite targets, with different dimensions and projectile material (steel) and target thicknesses

Table 3
Residual velocities comparison with data from Refs. [1,16].

Target material	Target thickness [mm]/n° layers	Projectile diameter [mm]	Projectile mass [g]	Experimental ballistic limit V_{50} [m/s]	Ballistic limit obtained from current analytical model [m/s]	Error [%]	Ballistic limit obtained from analytical model [1] [m/s]	Error [%]
E-glass-vinylester [1].	4.5/11	4.76	3.3	175	160	−8.5	190	+8.5
E-glass-vinylester [1].	4.5/11	6.35	3.84	210	185	−11.9	215	+2.3
E-glass-vinylester [16].	4.5/11	4.76	3.84	181	160	−11.6	190	+4.9
E-glass-vinylester [16].	9/22	4.76	3.84	291	257	−11.8	270	−7.4
E-glass-vinylester [16].	14/33	4.76	3.84	390	355	−9	320	−18
E-glass-vinylester [16].	19/44	4.76	3.84	501	460	−8.3	360	−28

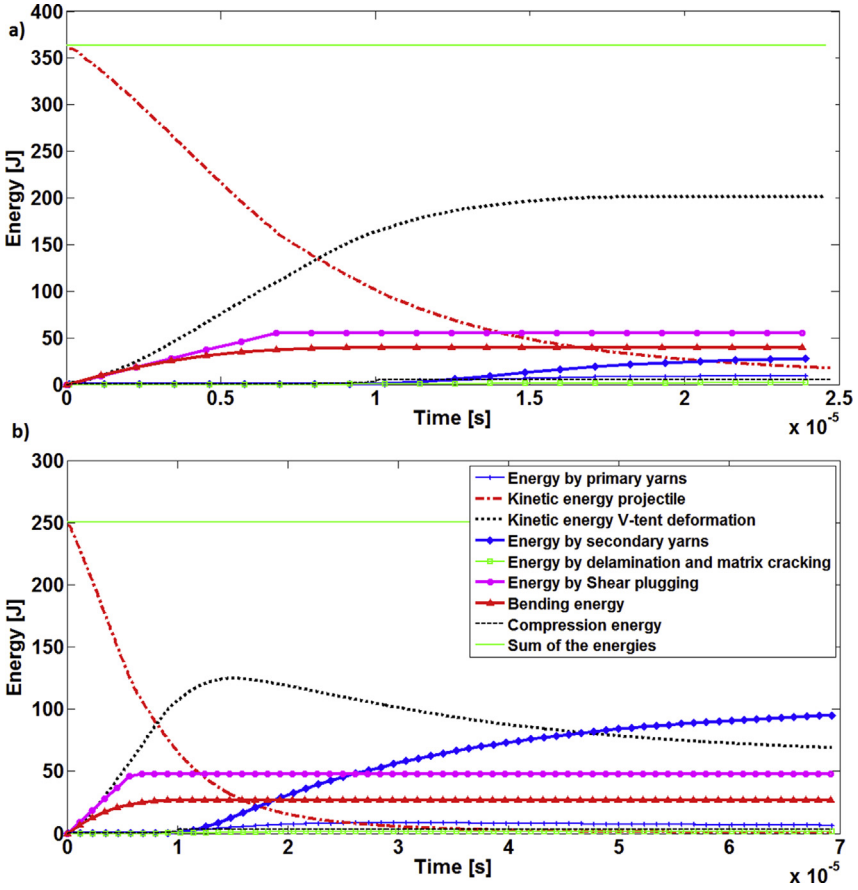

Fig. 7. a) 19 mm E-glass 470 m/s complete perforation, b) 19 mm E-glass 390 m/s partial perforation (30 failed).

(plain-weave fabrics). Table 2 contains the data for the target from Refs. [12,17,18].

In Table 3 the experimental and analytical data from the current model and the one developed according to [1] are compared. The results show that the present model, which implements bending, compression and sequential failure caused by the in-thickness longitudinal wave, fits the experimental results, excellently for both thin and thick targets. The gap between the results of the two analytical models actually increases for thick targets (over 10 mm) which are influenced to a greater degree by the bending energy. For thin targets, the present analytical model tends to underestimate the ballistic limit by a few percent, the opposite of what is evinced for Kevlar® analyses that predict a slightly higher ballistic limit. The current analytical model underestimates the ballistic limit by about 10% for all thicknesses of E-glass specimens. It therefore provides an excellent conservative prediction with regards to a protection design aim. With respect to the comparison with [5], in this case some parameters including the dimension of the yarns are unknown and therefore introduce an additional factor of uncertainty.

3.2. *Energy dissipation and morphological features*

In addition to the residual velocity of the projectile, the current analytical model provides several important outputs that allow deepening of the understanding of the impact phenomenon and also provides other parameters to judge the accuracy of the model itself, compared to the experimental results. In particular the evolution in time of the energy dissipated by the target gives an

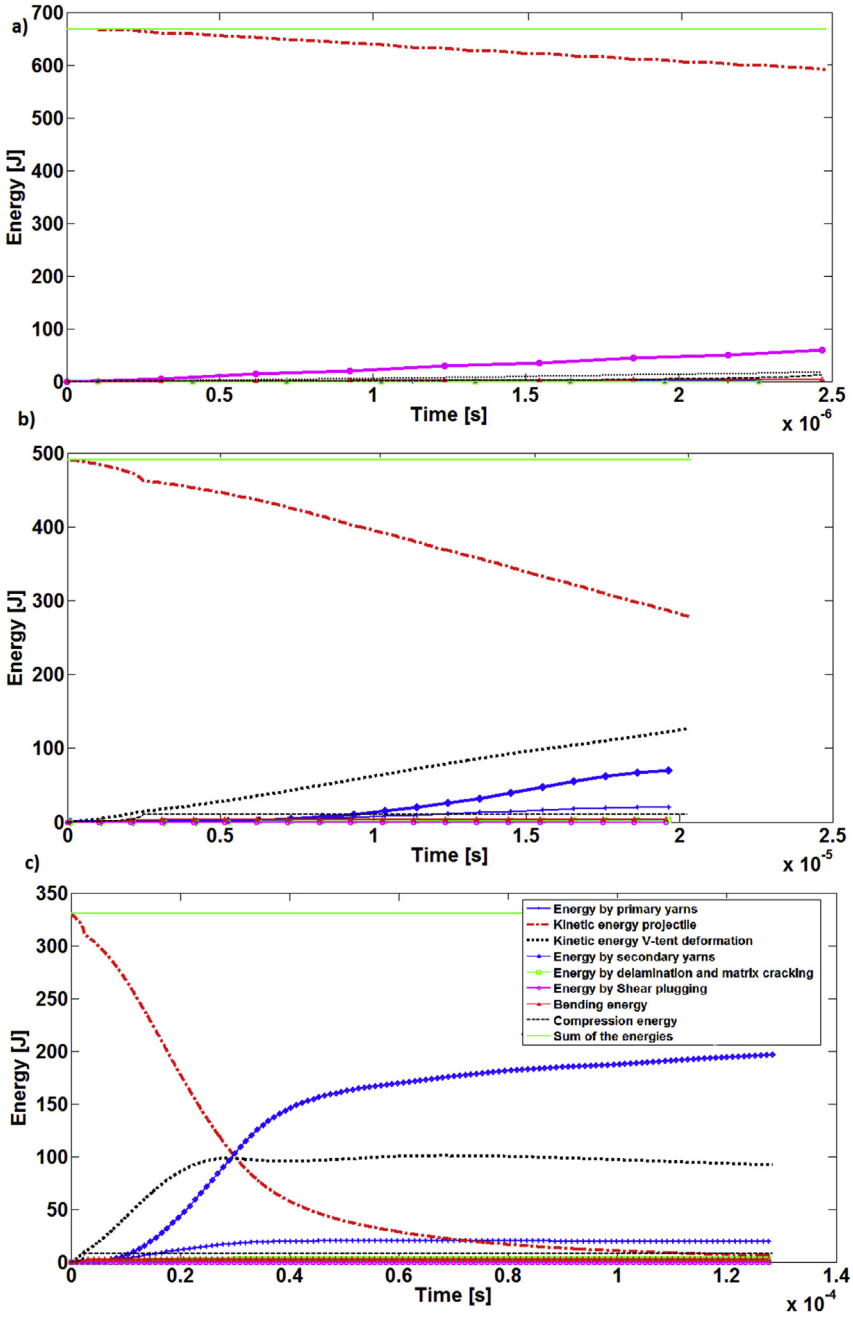

Fig. 8. a) 5 mm Kevlar®29 210 m/s complete shear plugging, b) 5 mm Kevlar®29 180 m/s complete perforation, c) 5 mm Kevlar®29 148 m/s partial perforation (10 failed).

indication of the central mechanisms in obtaining high performance ballistic protections. These dissipated energies are not easily comparable with experimental results, however some considerations can be made.

The comparison of Fig. 7 a) and b) brings out some important considerations: the contribution of the energy dissipated by bending is important for thick targets (in this case 19 mm E-glass), and represents approximately 15% of the initial kinetic energy of the projectile. E-glass fibres have a lower shear strength than Kevlar, and hence the contribution of the energy dissipated by shear plugging is relevant and important in the first instants when a strong growth of this phenomenon occurs, related to the failure of the first layers by this mechanism. When the target is completely perforated (see Fig. 7a), the contribution of tensile strain by primary and secondary yarns remains low because of their failure by shear plugging and tension. On the other hand, at lower velocity, with only partial perforation, the contribution of the energy absorbed by tension is high, but also in this case the secondary yarns dissipate more energy than the primary ones, even if the latter undergo the highest strain, because the number of secondary yarns is considerably greater. The compression energy, delamination and matrix cracking seem to contribute little. Finally, the kinetic energy absorbed by the "V-tent" deformation moving forward together with the projectile is the most relevant contribution and is related to the spread of the transverse waves that involve the motion of a large mass. These considerations are also in agreement with observations made in Ref. [1].

Fig. 8a), b) and c) show the energy trend of the Kevlar®29 target in three different situations: in Fig. 8a, all the layers undergo shear plugging and the target is completely perforated, with only a small reduction in the kinetic energy of the projectile. Shear plugging is the most relevant mode of energy dissipation and the duration of this phenomenon is short. This explains why at high impact speed the gap between the results of the two analytical models is small, since the dissipation by bending and other mechanisms related to sequential failure are negligible. In Fig. 8b the projectile has completely perforated the target without shear plugging, all the layers have failed in tension: the kinetic energy of the "V-tent" deformation is the most relevant, followed by the secondary yarns, while the others remain low. In Fig. 8c, there is partial perforation and the trend of the energies is similar to Fig. 7b, except for the bending energy that for the 5 mm target being lower, close to 1–2% of the initial energy, with delamination and matrix cracking being again minor influencing parameters.

Fig. 9a) and b) are enlargements of the energy trend for the 5 and 10 mm Kevlar® plates: the kinetic energy dissipated by the "V-

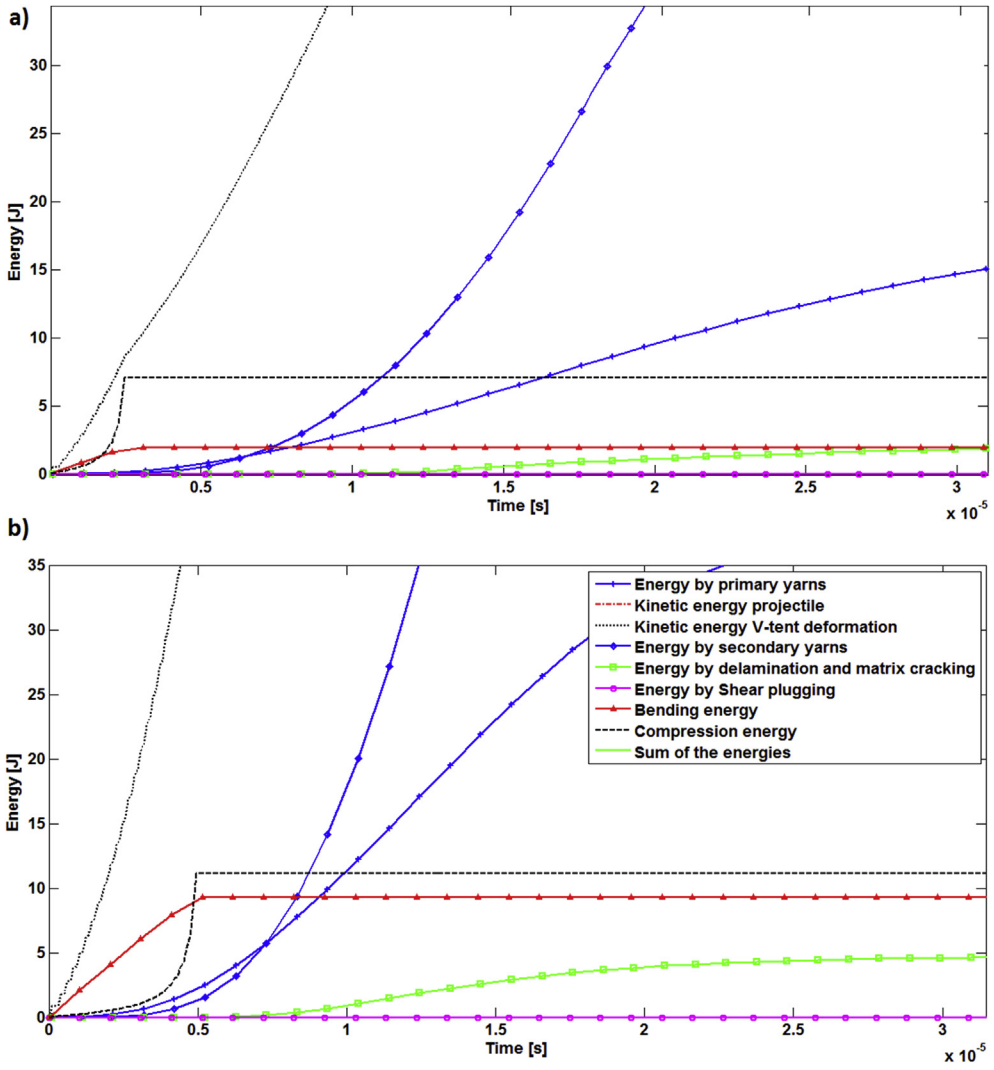

Fig. 9. a) 5 mm energy trend in the first instants, b) 10 mm energy trend in the first instants.

Table 4
Experimental and analytical dimensions of the "V-tent" deformation, number of failed layers.

# Test	Max "V-tent" radius R [mm]		Max "V-tent" depth Z [mm]		Number of failed layers	
	Experimental	Analytical	Experimental	Analytical	Experimental	Analytical
K5#1	63.3	85	21.8	5.4	2	0
K5#5	30	60	7.5	5.3	12	12
K5#7	27.6	16	9.5	2.9	12	12
K10#1	50	75	12.7	4.7	10	0
K10#3	41.2	85	11.5	5.8	24	24
K10#4	93	110	32	6.6	20	16
K10#6	38.5	15	14	3.2	24	24

tent" conoid clearly increases the fastest, underlining its important contribution in stopping the projectile. The other important contributions in the first instants are the compression and bending energy, overall for the 10 mm plate, in agreement with the results highlighted in Fig. 7 for the 19 mm E-glass specimens, where the contribution is also considerably higher. These analyses show that the energy dissipation is related overall to the kinetic energy absorbed by the "V-tent" deformation, the energy of yarns in tension and the bending energy and the compression for thick targets, especially in the first instants. Increasing the density of the material would allow an increase of the kinetic energy of the "V-tent" deformation but would decrease the velocity of the waves and hence the capability of the material to distribute energy over a wide area, and also the same "V-tent" kinetic energy would be penalized.

The analysis of the dimensions of the "V-tent" deformation at the moment of failure and the number of failed layers when partial penetration occurs, give a further validation of the model; these features have been compared with experimental data from Ref. [5]. Table 4.

The analytical model reproduces the number of failed layers quite well, also when incomplete perforation occurs; however it must be taken into account that this model is not able to reproduce the results variability related to manufacturing issues of the composite fabrics and especially to the impact yaw angle of the projectile, etc. The K5#1 simulation predicts no failed layers against two in the experimental test, which is an excellent result, like the K10#4 as well. The less accurate result is the K10#1, but the experimental test was affected by a high Yaw angle (14°), which means a better perforation capability of the projectile as explained in [5]. With regards to the dimension of the "V-tent" deformation, the model partially fails in reproducing the experimental values, most of all when predicting the depth of the conoid which is constantly predicted to be lower, while the radius prediction is more precise; the K5#7 and K10#6 analyses present a lower radius since the model predicted shear plugging, with a reduction of the spread of the transverse wave.

4. Conclusions

The improved analytical model presented in this paper aims to be an evolution of already existing ballistic models based on the energy balance of the projectile with different modes of dissipation available in composite targets. In particular, improvements have been carried out on the sequential failure of the layers after the impact of a blunt shaped projectile, on the energy dissipated by secondary yarns, on the compression energy and on the introduction of dissipation by means of bending of the plate. The comparison of the results obtained with the improved model with experimental tests from the authors [5] and with data from the literature [1,16] points out its increased reliability and precision, showing that the contribution of the bending energy becomes relevant for thick targets. Moreover, the model is able to give an insight into the behaviour of the impacted layers describing the failure of each single layer. This could be of interest for design purposes allowing a better understanding of the residual strength of a protective structure. This analytical model is aimed to be the first instrument in ballistic protection design, able to highlight a possible track for further optimization procedures that exploit numerical models and experimental tests. The study of the energy dissipation modes versus time, gives the possibility to investigate the different dissipation modes. Further room for improvement of the model exists through predicting the friction among the yarns and the delamination mode that currently exists only as a second mode delamination.

References

[1] Naik NK, Shrirao P, Reddy BCK. Ballistic impact behaviour of woven fabric composites: formulation. Int J Impact Eng 2006;32:1521–52.
[2] Morye SS, Hine PJ, Duckett RA, Carr DJ, Ward IM. Modelling of the energy absorption by polymer composites upon ballistic impact. Compos Sci Technol 2000;60:2631–42.
[3] Velmurugan R, Sikarwar RS, Gupta NK. Analytical modelling for ballistic perforation of angle-ply and hybrid composite laminates. In: Proceedings of the IMPLAST conference, 12–14 October. Rhode Island USA;Providence1-12: Society for Experimental Mechanics, Inc; 2010. p. 1–12.
[4] Vinson JR, Zukas JA. On the ballistic impact of textile body armour. J Appl Mech 1975;42:263–8.
[5] L.M. Bresciani, A. Manes, A. Ruggiero, G. Iannitti and M. Giglio, Experimental tests and numerical modelling of ballistic impacts against kevlar29 plain-woven fabrics with epoxy matrix: macro-homogenous and meso-heterogeneous approaches, Under Revis.
[6] Chen X, Zhu F, Wells G. An analytical model for ballistic impact on textile based body armour. Compos Part B 2013;45:1508–14.
[7] Roylance D. Ballistic of transversely impacted fibers. Text Res J 1977;47(10): 679–84.
[8] Field JE, Sun Q. High-speed photographic study of impact on fibres and woven fabrics. Proc SPIE 1991;1358:703–12.
[9] Smith JC, McCrackin FL, Schiefer HF. Stress-strain relationships in yarns subjected to rapid impact Loading: 5. Wave propagation in long textile yarns impacted transversely. J Res Natl Bureau Stand 1958;60(5):517–34.
[10] Roylance D, Wilde AF, Tocci GC. Ballistic impact of textile structures. Text Res J 1973;43(1):34–41.
[11] Naik NK, Doshi AV. Ballistic impact behaviour of thick composites: analytical formulation. AIAA J 2005;43(7):1525–36.
[12] Cunniff PM. An analysis of the system effects in woven fabrics under ballistic impact. Text Res J 1992;62(9):495–509.
[13] Naik NK, Shrirao P. Composite structures under ballistic impact. Compos Struct 2004;66:579–90.
[14] Gower HL, Cronin DS, Plumtree A. Ballistic impact response of laminated composite panels. Int J Impact Eng 2008;35:1000–8.
[15] Naik NK, Shrirao P, Reddy BCK. Ballistic impact behaviour of woven fabric composites: parametric studies. Material Sci Eng A 2005;412:104–16.
[16] Gellert EP, Cimpoeru SJ, Woodward RL. A study of the effect of target thickness on the ballistic perforation of glass-fibre-reinforced plastic composites. Int J Impact Eng 1999;24:445–56.
[17] Deka LJ, Bartus SD, Vaidya UK. Damage evolution and energy absorption of E-glass/polypropylene laminates subjected to ballistic impact. J Mater Sci 2008;43:4399–410.
[18] Kollàr LP, Springer GS. Mechanics of composite structures. Appendix C: typical material properties. Cambridge University Press; 2003. p. 464–7. Printed in the United Kingdom at the University Press, Cambridge, ISBN 0 521 80165 6 hardback.